Size-dependent magnetic properties of nickel nanochains

2007 J. Phys.: Condens. Matter 19 036216

(http://iopscience.iop.org/0953-8984/19/3/036216)

INSTITUTE OF PHYSICS PUBLISHING JOURNAL OF PHYSICS: CONDENSED MATTER

J. Phys.: Condens. Matter **19** (2007) 036216 (10pp) doi:10.1088/0953-8984/19/3/036216

Size-dependent magnetic properties of nickel nanochains

Lin He[1], Wangzhi Zheng[1], Wei Zhou[2], Honglin Du[1], Chinping Chen[1] and Lin Guo[2]

[1] Department of Physics, Peking University, Beijing 100871, People's Republic of China
[2] School of Materials Science and Engineering, Beijing University of Aeronautics and Astronautics, Beijing 100083, People's Republic of China

E-mail: cpchen@pku.edu.cn and guolin@buaa.edu.cn

Received 7 October 2006, in final form 8 December 2006
Published 5 January 2007
Online at stacks.iop.org/JPhysCM/19/036216

Abstract

Magnetic properties with three different sizes of Ni nanochains, synthesized by a technique of wet chemical solution, have been investigated experimentally. The sample sizes (average diameter of the nano-particles) are 50, 75, and 150 nm, with a typical length of a few microns. The characterizations by XRD and TEM reveal that the samples consist of Ni nano-particles forming a one-dimensional (1D) chain-like structure. Magnetic properties have been investigated by temperature dependent magnetization $M(T)$ and field dependent magnetization $M(H)$ measurements. The results are explained within the context of the core–shell model. First, the freezing of disordered spins in the shell layer has resulted in a peak structure on the zero-field-cooled (ZFC) $M(T)$ curve. The peak position is identified as the freezing temperature T_F. It is well described by the de Almeida–Thouless (AT) equation for the surface spin glass state. Second, the shape anisotropy of the 1D structure has caused a wide separation between the field-cooled (FC) and ZFC $M(T)$ curves. This is mainly attributed to the blocking of the core magnetism by an anisotropy barrier, E_A. Third, by the $M(H)$ measurement in the low field region, the open hysteresis loop measured at $T = 5$ K $< T_F$ is significantly enlarged in comparison with that taken at $T > T_F$. This indicates that a significant part of the contribution to the magnetic irreversibility at $T < T_F$ is arising from the disordered spins in the shell layer. Last, with the reduced sample size, the coercivity, H_C, increases whereas the saturation magnetization goes down substantially. These imply that, as the sample size reduces, the effect of shape anisotropy becomes larger in the magnetization reversal process and the contribution to the magnetism from the ferromagnetically ordered core becomes smaller.

1. Introduction

In recent years, nano-scaled magnetic materials have received much attention, due to the fundamental interest in their unique magnetic properties in comparison with those of the bulk phase and to their promising application potential in technology such as in high-density magnetic storage, etc. Their magnetic properties are usually dictated by the size, dimension, shape, structure, and morphology of the constituent phases, along with the type and strength of magnetic coupling. Various magnetic nano-structures have been synthesized using different techniques, for example, Co/Ni nanorods via chemical solution [1] or physical vapour-phase epitaxy [2], hollow Ni nanospheres with diameter of 300–450 nm via a chemical method [3], Ni growing on peptide nanotubes [4], Ni complex nanotubes having diameter of 20–40 nm and length of 2 μm [5], and Co_3O_4 porous nanotubes with diameter ranging from tens to 200 nm and sidewall thickness ranging from 2 to 20 nm [6]. By virtue of these novel ferromagnetic nanostructures, people increasingly have deeper understanding of their magnetic properties and potential applications. Intensive investigation has been devoted to demonstrate the enhanced anisotropy on the nano-scaled magnetic material, especially in one or two dimensions [7], and to study the behaviour of the spin disorder state in the surface or boundary layer [8–10], or in the metal–insulator multilayer [11].

Some experiments have reported that the saturation magnetic moment reduces with decreasing size [8, 12, 13], while others reported the same value as in the bulk phase [14]. By contrast, experiments performed on the Fe, Co, and Ni clusters in a molecular beam have demonstrated that the magnetic moment is atom-like, i.e. larger than the bulk value, with the cluster size less than 30 atoms. It decreases, approaching the bulk limit as the particle size increases to 700 atoms or so [15]. These seemingly conflicting results indicate that the saturation magnetization of nano-particles depends not only on the magnitude of the individual atom or spin moment, but also on the particle size or the complicated surface condition of the particle.

Recently, the core–shell model has been applied to describe the magnetic properties of a nanoparticle with a single crystal phase. In this case, it refers to a particle with a surface spin glass layer and a magnetically ordered core. For example, the surface spin glass state with $NiFe_2O_4$ [8], Fe_3O_4 [16], and $MnFe_2O_4$ nanoparticles [17] has been studied by applying this model. In this sense, the magnetic structure is divided into two major components. The core refers to the inner part of a nanoparticle that exhibits bulk-like magnetic ordering, and the shell layer refers to a spin-glass surface state. As the particle size reduces, the magnetic property of the surface layer is expected to become increasingly important due to the growing surface-to-volume ratio.

Very recently, pure Ni nanospheres connected with each other forming chain-like structures have been synthesized by a wet chemical route [18]. By controlling the reaction conditions, we successfully obtain the constituent nanospheres with different diameters, ranging from 50 to 150 nm. This provides a unique model system for the fundamental investigation into the magnetism associated with the surface spin, the variation of magnetism with the sample size, and the magnetization reversal mechanism with the quasi-1D nanostructure. The thermal behaviour of the magnetization, $M_{FC}(T)$ and $M_{ZFC}(T)$ by the FC and ZFC measurements, has exhibited two major features. One is a peak in the $M_{ZFC}(T)$ curve at low temperature. It is identified as the freezing temperature, T_F, ascribed to the freezing of surface moments. The other is a broad maximum observed with the $M_{ZFC}(T)$ curve in the high temperature region. It is identified as the blocking temperature, T_B, attributed to the presence of an anisotropy barrier, E_A. The field dependent measurements $M(H)$ at different temperatures show that the saturation magnetization reduces with the reduced particle size. The coercivity

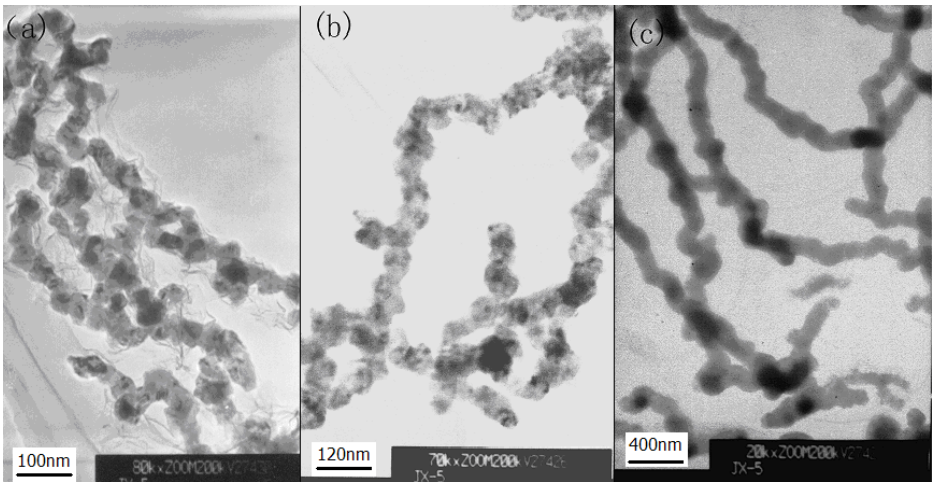

Figure 1. TEM images of the nanochains. (a) Nickel chains with sphere diameter ∼50 nm. They are capped with residual PVP. (b) Nickel chains, ∼75 nm, with uniform structure. (c) Nickel chains, ∼150 nm.

of a 50 nm nickel nanochain has been determined experimentally at various temperatures. It reveals an important contribution arising from the surface magnetic state to the irreversibility of magnetization reversal.

2. Sample preparation and characterization

Synthesis of the sample has been performed by a wet chemical route, the same as that in our previous report [18]. The chain-like structure is formed by a self-assembly process of Ni nanospheres with the modification of a multidentate ligand, polyvinyl pyrrolidone (PVP), on the surface. The PVP is known to have no magnetism. Three different sizes of nano-chain are obtained, 50, 75, and 150 nm, labelled as S50, S75, and S150, respectively. The size distribution is about 10 nm. The samples have a typical length of a few micrometres. Typical TEM images of the S50, S75, and S150 samples are shown in figure 1. The Ni nano-particles are structurally connected together, forming chain-like networks. In figure 1(a), the residual PVP is vaguely visible surrounding the Ni chain, while in figures 1(b) and (c) no sign of PVP encapsulation is visible. To further investigate the mass effect of the nonmagnetic PVP on the magnitude of the magnetization, thermogravimetry (TG) has been performed on the three samples using a Perkin Elmer thermogravimeter (Diamond TG/DTA). The relative weight loss corresponding to the residual PVP is determined as 22.6%, 10.9%, and almost 0% for S50, S75, and S150, respectively. This correction factor on the magnetization due to the mass effect of the PVP has been accounted for in the determination of the magnetization.

Figure 2 shows XRD patterns for S50, S75, and S150. The main peaks, which are indexed with the S150 curve representative for all of the three samples, correspond to the face centred cubic (fcc) nickel (JCPDS 04-0850). The remaining weak peaks marked with stars on the S50 curve conform to the crystal planes of nickel carbide, Ni_3C (JCPDS77-0194). The surface carbonization of the nickel nano-chains occurred during the preparation process, leading to the formation of Ni_3C probed in the XRD measurement. The peaks corresponding to Ni_3C in S50 are a little stronger than the ones in S75. This further proves that Ni_3C indeed exists at

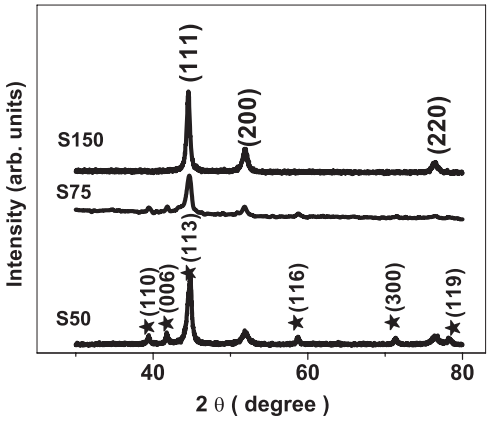

Figure 2. XRD patterns for S50, S75, and S150. The main peaks are indexed to pure fcc nickel (JCPDS 04-0850). The remaining asterisked weak peaks, more obviously visible for S50, conform to the crystal planes of nickel carbide, Ni_3C, with a trigonal system (JCPDS77-0194).

the surface, since S50 has a larger surface to volume ratio, which causes a higher fraction of the carbonized atoms. Comparing with the XRD pattern of S50 or S75, the peaks appearing in the S150 curve can be easily indexed to the pure fcc nickel (JCPDS 04-0850). No peak corresponding to Ni_3C in the curve for S150 has been observed. Perhaps this is because the amount of Ni_3C with S150 is beyond the sensitivity of XRD measurement.

3. Magnetic measurements and analysis

Magnetic measurements on the powdered samples have been performed using a SQUID magnetometer (Quantum Design). $M(T)$ curves are recorded in an applied field, $H_{\rm app} = 90$ Oe, in increasing temperature after the sample cooling with FC and ZFC modes. By the FC mode, the sample was first cooled down to the lowest temperature in a cooling field, $H_{\rm COOL} = 20$ kOe, before the data recording. In addition, the $M_{\rm ZFC}(T)$ for S50 are recorded in various applied fields from 90 Oe to 1 kOe to investigate the effect of field strength on the magnetization state. The corresponding field dependence of the freezing temperature, $T_{\rm F}(H_{\rm app})$, and blocking temperature, $T_{\rm B}(H_{\rm app})$, are analysed. Also, $M(H)$ measurements at $T = 5$, 300, and 380 K are performed to study the size effect on the saturation magnetization and the coercivity.

3.1. $M_{ZFC}(T)$ and $M_{FC}(T)$ measurements in a recording field of 90 Oe

For all three samples, the $M_{\rm FC}(T)$ and $M_{\rm ZFC}(T)$ curves separate from each other with the temperature going up to 395 K, as shown in figure 3. It indicates the presence of an anisotropy barrier, $E_{\rm A}$, which is mainly attributed to the shape anisotropy of the 1D structure. The behaviour of $M(T)$ curves reveals the main feature of thermal activation effect against the barrier, $E_{\rm A}$, i.e., $M_{\rm ZFC}(T)$ increases and $M_{\rm FC}(T)$ decreases with increasing temperature. In the low temperature region, $M_{\rm ZFC}(T)$ exhibits a peak structure at about 13 K; see the inset of figure 3. There is no obvious dependence of the peak position on the sample size. The peak height, however, increases with the reduced sample size. This suggests that it is resulting from the defreezing of the frozen moment in the surface layer. The peak temperature is defined as the freezing temperature, $T_{\rm F}$.

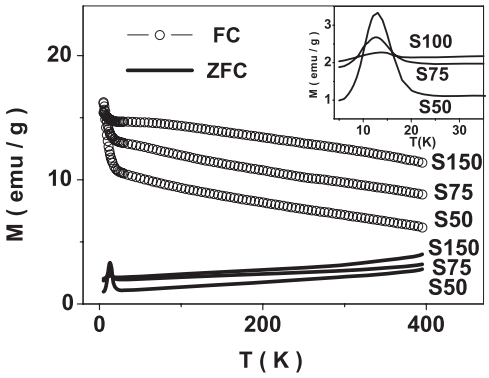

Figure 3. FC and ZFC $M(T)$ measurements recorded in $H_{app} = 90$ Oe. The measurement is performed from $T = 5$ to 395 K. For the FC measurement, the cooling field is 20 kOe. The inset shows M_{ZFC} in the low temperature region. The peak position around 13 K is the freezing temperature, T_F.

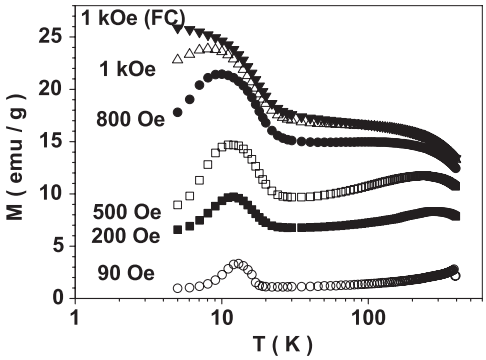

Figure 4. $M_{ZFC}(T)$ for the S50 sample. ZFC data recorded in $H_{app} = 90$, 200, 500, 800 Oe, and 1 kOe. The FC curve measured in 1 kOe is included. The $M_{ZFC}(T)$ and $M_{FC}(T)$ curves recorded in 1 kOe merge at about $T = 50$ K.

3.2. $M_{ZFC}(T)$ measurements for S50 in various recording fields

In order to further investigate the effect of the applied field on the blocking and freezing property of the sample, the $M_{ZFC}(T)$ curves for S50 have been recorded in the fields of 90, 200, 500, 800 Oe and 1 kOe. The FC curve measured in 1 kOe is included as well for the purpose of comparison. These results are plotted in figure 4. As the applied field for the measurement increases, a broad maximum becomes more obvious in the high temperature region with the $M_{ZFC}(T)$ curves. This is owing to the effect of thermal activation with the core magnetism against the anisotropy barrier, E_A. The blocking temperature, $T_B(H_{app})$, is defined by the position of the maximum in the curve. As H_{app} increases, T_B moves toward the low temperature end, and eventually vanishes by the applied field of 1 kOe. The ZFC and FC curves almost coincide with each other in the applied field, $H_{app} = 1$ kOe, except in the low temperature region, $T < 10$ K, where $M_{ZFC}(T)$ still exhibits a peak showing the freezing property. The freezing temperature, T_F, shifts down slightly with the progressively increasing applied magnetic field.

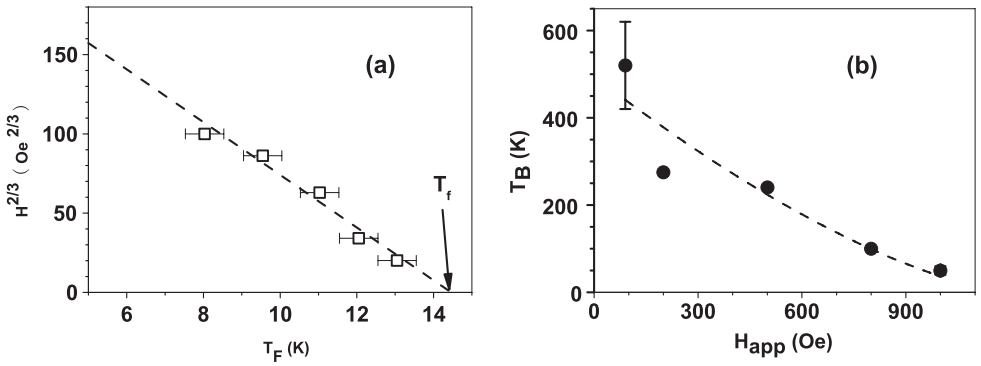

Figure 5. Field dependence of the freezing temperature, T_F, and the blocking temperature, T_B for S50. (a) External field versus freezing temperature. The dashed line represents the fitting result by the de Almeida–Thouless equation. (b) Blocking temperature versus external field. The dashed curve is for the fitting by equation (2). The anisotropy constant obtained from the fitting is $K \sim 5.6 \times 10^4$ J m^{-3}.

3.3. Freezing and blocking temperatures with S50

The detailed investigation into S50 clearly shows that the surface spins lead to a typical freezing behaviour at low temperature. It gives rise to the peak structure around 13 K shown in figure 4. The relation between the freezing temperature, T_F, and the corresponding external applied field, $H_{app} = H_{AT}$, can be described by the de Almeida–Thouless (AT) equation, see for example [9, 16],

$$H_{AT}(T_F)/\Delta J \propto \left(1 - \frac{T_F}{T_f}\right)^{3/2} \tag{1}$$

where T_f is a fitting parameter representing the freezing temperature in a vanishing magnetic field and ΔJ is the width of the distribution of exchange interaction. The plot for the freezing temperature versus the external field is illustrated in figure 5(a). The error bars represent the uncertainty in determining T_F. It is 0.5 K for each point, determined by the step size in temperature. The dashed line represents the fitting result by the AT equation. It goes through the data points, showing a reasonably good fitting. The $H^{2/3}$ dependence demonstrates the 'surface' spin-glass behaviour, which is different from the $H^{1/2}$ dependence for a 'volume' spin-glass behaviour as discussed in [16]. The zero-field freezing temperature is obtained by extrapolation in figure 5(a) as $T_f = 14.5$ K.

Besides the freezing temperature, T_F, for the surface magnetism obtained from figure 4(a), the blocking temperature, T_B, for the core magnetism can also be determined from the broad maximum in the high temperature region of the $M_{ZFC}(T)$ curves. It is plotted versus the applied field in figure 5(b). In the case of $H_{app} = 90$ Oe, $M_{ZFC}(T)$ does not reach the maximum within the range of measurement. Hence, T_B should occur between 400 K and the Curie point of Ni, ~630 K. It is therefore reasonable to estimate the value as 520 ± 100 K. Furthermore, by extrapolation of the $M_{ZFC}(T)$ and $M_{FC}(T)$ curves for S50 in figure 3, the intersection is expected to fall within this estimated value. On the other hand, $M_{ZFC}(T)$ does not show any maximum with $H_{app} = 1$ kOe except for the freezing peak at T_F. One can estimate T_B by the criterion that it is close to the temperature where FC and ZFC merge, $\sim 50 \pm 10$ K. A simple equation based on the analysis of Neel [19] and Brown [20] for the blocking temperature, see for example [21], is applied to fit these points,

$$T_B(H_{app}) = \frac{KV}{k_B \ln(\tau_{obs}/\tau_0)}\left(1 - \frac{H_{app}}{H_K}\right)^{3/2} \quad (2)$$

where H_K is a fitting parameter for the anisotropy field at zero temperature, K is the anisotropy constant, V is the switching volume, τ_{obs} is the experimental observation time interval, and τ_0 is the characteristic time constant, usually in the range of 10^{-9}–10^{-11} s. The exponent 3/2 is for a collection of randomly oriented powdered samples with magnetization reversal by nucleation rotation [22]. This is reasonable given that the coherence length of Ni is about 25 nm [23]. When applying equation (2), we use $\ln(\tau_{obs}/\tau_0) = 25$, $M_S = 485$ emu cm^{-3} (bulk value of Ni). The fitting result is presented in figure 5(b) by the dashed curve. The anisotropy field at zero temperature H_K is obtained from the fitting as 1.1 kOe, and the anisotropy energy barrier at zero field expressed in units of thermal energy k_BT is $E_A = KV \sim 12\,370$ K. The value of energy barrier is similar to the experiment on a single Ni nanowire with diameter from 40 to 100 nm and length up to 5 μm, $E_A \sim 15\,000$ K [24]. For randomly oriented samples, the anisotropy field can be expressed as $H_K = 0.96K/M_S$ [25]. By using the values of H_K and M_S mentioned above, the anisotropy constant K is then estimated as $\sim 5.6 \times 10^4$ J m^{-3}, which is one order of magnitude larger than the value of magnetocrystalline anisotropy of bulk phase, $\sim 4.5 \times 10^3$ J m^{-3}. This large anisotropy is probably attributable to the shape anisotropy of the 1D chain. It is worth noting that the value of $H_K \sim 1.1$ kOe is in consistence with the result of $M(T)$ measurements shown in figure 4, in which the $M_{ZFC}(T)$ and $M_{FC}(T)$ curves almost coincide with each other under the applied field, $H_{app} = 1$ kOe. The demagnetization factor, $\Delta N \sim 0.19$, is calculated according to the expression $K = 1/2\ \mu_0 \Delta N M_S^2$. This value is similar to those of 1D Fe, Co, and Ni nanowires with magnetization reversal by nucleation rotation [26]. From the result determined from the fitting, $E_A = KV \sim 12\,370$ K, with the value of K already determined, the effective switching volume V is estimated as $(14.5\ \text{nm})^3$. It is nearly two orders smaller than the volume of a single nanosphere in the nanochain, i.e. $D \sim 50$ nm with S50. This feature is also similar to the experiment on a single Ni nanowire with diameter from 40 to 100 nm and length up to 5 μm. The switching volume is obtained as $(20\ \text{nm})^3$, also smaller than the particle volume by two orders of magnitude [24].

3.4. $M(H)$ measurements

The $M(H)$ measurements at $T = 5$, 300 and 380 K for S50 are plotted in figure 6. The loop measured at $T = 5$ K $< T_F$ is much more pronounced in comparison with the ones measured at high temperatures. This indicates an important contribution arising from the surface magnetism. Similar enhancement on the hysteresis loop attributed to the surface magnetism arising from the uncompensated AFM spins at $T < T_F$ has been reported with the nano-composite, $(Cu)_{core}/(Cu_2O + CuCl + \text{minute}CuO)_{shell}$ [27]. The saturation magnetizations determined in the high field region, ~50 kOe, see the inset, are 44.4 emu g^{-1} (5 K), 19.4 emu g^{-1} (300 K), and 16.5 emu g^{-1} (380 K), corresponding to effective moments of 0.47 μ_B, 0.20 μ_B, and 0.17 μ_B per Ni atom, respectively. This is much smaller than the listed bulk value of 0.606 μ_B per Ni atom at 300 K. The much enhanced moment obtained at $T < T_F$ in comparison with that at $T > T_F$ suggests that the surface magnetism is indeed very important for the nano-sized particles. This is consistent with the results obtained by the $M_{ZFC}(T)$ and $M_{FC}(T)$ measurements.

The $M(H)$ measurements have also been carried out for S75 and S150. The corresponding saturation magnetizations and the coercivity are summarized in table 1. The larger the sample size, the larger the saturation magnetization. For S150 at 300 K, the value is 47.5 emu g^{-1}, reaching 83% of the bulk limit. This suggests that the magnetism starts deviating from the bulk value at the sample size around 150 nm or so. On the other hand, the coercivity reduces with

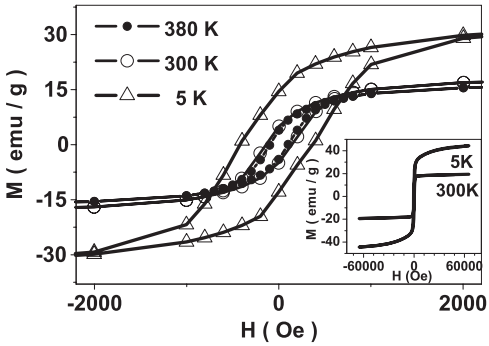

Figure 6. Hysteresis loops measured at $T = 5$, 300 and 380 K. The inset gives the results in the saturation region.

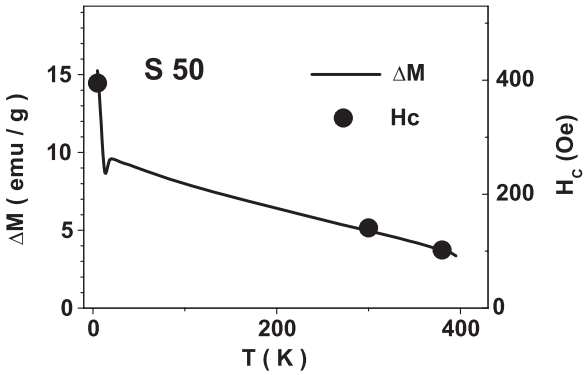

Figure 7. Difference in the magnetization between $M_{\mathrm{ZFC}}(T)$ and $M_{\mathrm{FC}}(T)$ measurements, $\Delta M = M_{\mathrm{FC}} - M_{\mathrm{ZFC}}$, with $H_{\mathrm{app}} = 90$ Oe. The right Y-axis is for the coercivity.

Table 1. Saturation magnetization and coercivity for S50, S75 and S150 at $T = 5$, 300 and 380 K, respectively.

	M_{S} (5 K)		M_{S} (300 K)		M_{S} (380 K)		H_{C} (Oe)		
	(emu g^{-1})	μ_{B}/Ni	(emu g^{-1})	μ_{B}/Ni	(emu g^{-1})	μ_{B}/Ni	5 K	300 K	380 K
S50	44.4	0.47	19.4	0.20	16.5	0.17	392	139	97
S75	48.9	0.52	36.9	0.39	33.6	0.35	305	124	112
S150	54.2	0.57	47.5	0.50	42.0	0.44	195	102	82

the increasing sample size. In figure 7, the coercivity, H_{C}, determined from the loops shown in figure 6 is plotted along with $\Delta M = M_{\mathrm{FC}} - M_{\mathrm{ZFC}}$ for S50. These two exhibit a proportional relation. It further reveals the important correlation of the surface magnetism with the hysteresis loop.

4. Discussion

The isothermal time relaxation of the ZFC magnetization for S50 has been measured at $T = 5$, 50, and 100 K with $H_{\mathrm{app}} = 200$ Oe. Using the simple equation, $M(t) = M_1 + M_2(1 - \mathrm{e}^{-t/\tau})$,

to approximate the relaxation behaviour, then, M_2/M_{ZFC} accounts for only 5% at 5 K, 1.2% at 50 K, and 2% at 100 K, with the measuring time of 2 h. Hence, the FC and ZFC data represent a reasonable approximation to the equilibrium value.

The magnetism of Ni_3C phase and the effect of carbon encapsulation on pure Ni has been investigated previously [28, 29]. The results in [30] indicate that the perfect crystalline Ni_3C is expected not to have ferromagnetism. Nevertheless, because of the defects in the crystal or the less coordination between C and Ni atoms, the Ni_3C sample exhibits a very weak ferromagnetic behaviour. Since the possibly existing magnetism of Ni_3C is weak and the amount of Ni_3C in our sample is insignificant, its magnetic effects can be neglected. The magnetic properties of the Ni phase are, therefore, not affected in the presence of a little nickel carbide phase detected by the XRD in figure 2.

In our experiment, the saturated magnetization decreases with the size of the nanochains. It is seriously reduced from the bulk value with S50. When comparing with some of the previously reported results mentioned in the introduction, we find that, in the cases with the reduced magnetization, the samples are not 'bare'. In [8], oleic acid (organic surfactant) is tightly bonded to the surface of $NiFe_2O_4$ powder. In [12], the Co nanoparticles are embedded in an amorphous matrix of Al_2O_3. Particularly, the chemical bonding between the organic compound and the surface magnetic atoms is very likely to quench the surface magnetic moments and contributes to the reduction of saturation magnetization. This has been observed in the experiment on the Ni carbonyl clusters of a few hundred atoms in which the magnetic moments was quenched by the chemical bonding [31]. In our experiment, the nanochain is capped with PVP. Perhaps, this is the reason for the modification of the surface magnetism. On the other hand, in the cases where the saturated magnetization remains or increases, the samples are bare. In other words, they are not encapsulated by other substances. Although the effect of encapsulation on the magnetization is a conjecture at this stage without any firm experimental support, the effect of surface magnetic state is obviously significant in the present work. It would be important in the future to further investigate the effect of different encapsulation materials on the surface magnetic state.

5. Conclusion

We have performed magnetic measurements on Ni nanochains with sizes of 50, 75, and 150 nm. Detailed investigations on S50 have revealed the freezing and blocking properties attributed to the surface magnetic state and the core magnetism, respectively. These magnetic properties are explained based on the core–shell model. In the core, the magnetic properties are similar to those of the bulk phase, except for the enhanced anisotropy due to the quasi-one-dimensional chain structure. In the surface layer, the spins exhibit spin-glass behaviour, which makes an enhanced contribution to the observed magnetism, e.g. enhanced saturation magnetization and coercivity, at $T < T_F$ in comparison with those obtained at $T > T_F$. A size-dependent effect exists on the observed magnetic properties. This can also be explained within the framework of the core–shell model.

Acknowledgments

Authors acknowledge the support from the National Natural Science Foundation of China (No 20673009), the programme for New Century Excellent Talents in the University (NCET-04-0164) and the Specialized Research Fund for the Doctoral Program of Higher Education (SRFDP-2006006005).

References

[1] Puntes V F, Krishnan K M and Alivisatos A P 2001 *Science* **291** 2115
[2] Jung S W, Park W I, Yi G-C and Kim M Y 2003 *Adv. Mater.* **15** 1358
[3] Bao J C, Liang Y Y, Xu Z and Si L 2003 *Adv. Mater.* **15** 1832
[4] Yu L T, Banerjee I A, Shima M, Rajan K and Matsui H 2004 *Adv. Mater.* **16** 709
[5] Guo L, Liu C M, Wang R M, Xu H B, Wu Z Y and Yang S H 2004 *J. Am. Chem. Soc.* **126** 4530
[6] Wang R M, Liu C M, Zhang H Z, Chen C P, Guo L, Xu H B and Yang S H 2004 *Appl. Phys. Lett.* **85** 2080
[7] Skomski R 2003 *J. Phys.: Condens. Matter* **15** R841
[8] Kodama R H, Berkowitz A E, McNiff E J Jr and Foner S 1996 *Phys. Rev. Lett.* **77** 394
[9] Martínez B, Obradors X, Balcells Ll, Rouanet A and Monty C 1998 *Phys. Rev. Lett.* **80** 181
[10] Bonetti E, Bianco L D, Fiorani D, Rinaldi D, Caciuffo R and Hernando A 1999 *Phys. Rev. Lett.* **83** 2829
[11] Sahoo S, Petracic O, Kleemann W, Stappert S, Dumpich G, Nordblad P, Cardoso S and Freitas P 2003 *Appl. Phys. Lett.* **82** 4116
[12] Luis F, Torres J M, García L M, Bartolomé J, Stankiewicz J, Petroff F, Fettar F, Maurice J-L and Vaures A 2002 *Phys. Rev.* B **65** 094409
[13] Szpunar B, Erb U, Palumbo G, Aust K T and Lewis L J 1996 *Phys. Rev.* B **53** 5547
[14] Uhm Y R, Park J H, Kim W W, Cho C-H and Rhee C K 2004 *Mater. Sci. Eng.* B **106** 224
[15] Billas I M L, Chatelain A and de Heer W A 1994 *Science* **265** 1682
[16] Wang H, Zhu T, Zhao K, Wang W N, Wang C S, Wang Y J and Zhan W S 2004 *Phys. Rev.* B **70** 092409
[17] Muroi M, Street R, McCormick P G and Amighian J 2001 *Phys. Rev.* B **63** 184414
[18] Liu C M, Guo L, Wang R M, Deng Y, Xu H B and Yang S H 2004 *Chem. Commun.* 2726
[19] Néel L 1949 *Ann. Geophys.* **5** 99
[20] Brown W F 1963 *Phys. Rev.* **130** 1677
[21] Nunes W C, Socolovsky L M, Denardin J C, Cebollada F, Brandl A L and Knobel M 2005 *Phys. Rev.* B **72** 212413
[22] Victora R H 1989 *Phys. Rev. Lett.* **63** 457
[23] Sellmyer D J, Zheng M and Skomski R 2001 *J. Phys.: Condens. Matter* **13** R433
[24] Wernsdorfer W, Hasselbach K, Benoit A, Barbara B, Doudin B, Meier J, Ansermet J-Ph and Mailly D 1997 *Phys. Rev.* B **55** 11552
[25] Bozorth R M 1956 *Ferromagnetism* (Princeton, NJ: Van Nostrand-Reinhold) p 831
[26] Paulus P M, Luis F, Kroll M, Schmid G and de Jongh L J 2001 *J. Magn. Magn. Mater.* **224** 180
[27] Li Q, Zhang S-W, Zhang Y and Chen C P 2006 *Nanotechnology* **17** 4981
[28] Sun X-C and Dong X-L 2002 *Mater. Res. Bull.* **37** 991
[29] Jamet M, Wernsdorfer W, Thirion C, Mailly D, Dupuis V, Mélinon P and Pérez A 2001 *Phys. Rev. Lett.* **86** 4676
[30] Yue L P, Sabiryanov R, Kirkpatrick E M and Leslie-Pelecky D L 2000 *Phys. Rev.* B **62** 8969
[31] van Leeuwen David A, van Ruitenbeek J M, de Jongh L J, Ceriotti A, Pacchioni G, Häberlen O D and Rösch N 1994 *Phys. Rev. Lett.* **73** 1432